molecules

MDPI

Article

New Pyranone Derivatives and Sesquiterpenoid Isolated from the Endophytic Fungus *Xylaria* sp. Z184

Yan Zhang [1,†], Yang Jin [1,†], Wensi Yan [1], Peishan Gu [1], Ziqian Zeng [1], Ziying Li [2], Guangtao Zhang [2], Mi Wei [3] and Yongbo Xue [1,*]

[1] School of Pharmaceutical Sciences (Shenzhen), Shenzhen Campus of Sun Yat-sen University, Shenzhen 518107, China; zhangy2328@mail2.sysu.edu.cn (Y.Z.); jiny67@mail2.sysu.edu.cn (Y.J.); yanws3@mail2.sysu.edu.cn (W.Y.); gupsh@mail2.sysu.edu.cn (P.G.); zengzq8@mail2.sysu.edu.cn (Z.Z.)
[2] School of Pharmacy, Binzhou Medical University, Yantai 264003, China; 15853386606@163.com (Z.L.); greatzhangtao@hotmail.com (G.Z.)
[3] School of Agriculture, Shenzhen Campus of Sun Yat-sen University, Shenzhen 518107, China; weim29@mail.sysu.edu.cn
* Correspondence: xueyb@mail.sysu.edu.cn
† These authors contributed equally to this work.

Abstract: The fungus *Xylaria* sp. Z184, harvested from the leaves of *Fallopia convolvulus* (L.) Á. Löve, has been isolated for the first time. Chemical investigation on the methanol extract of the culture broth of the titles strain led to the discovery of three new pyranone derivatives, called fallopiaxylaresters A–C (**1**–**3**), and a new bisabolane-type sesquiterpenoid, named fallopiaxylarol A (**4**), along with the first complete set of spectroscopic data for the previously reported pestalotiopyrone M (**5**). Known pyranone derivatives (**6**–**11**), sesquiterpenoids (**12**–**14**), isocoumarin derivatives (**15**–**17**), and an aromatic allenic ether (**18**) were also co-isolated in this study. All new structures were elucidated by the interpretation of HRESIMS, 1D, 2D NMR spectroscopy, and quantum chemical computation approach. The in vitro antimicrobial, anti-inflammatory, and α-glucosidase-inhibitory activities of the selected compounds and the crude extract were evaluated. The extract was shown to inhibit nitric oxide (NO) production induced by lipopolysaccharide (LPS) in murine RAW264.7 macrophage cells, with an inhibition rate of 77.28 ± 0.82% at a concentration of 50 μg/mL. The compounds **5**, **7**, and **8** displayed weak antibacterial activity against *Staphylococcus areus* subsp. *aureus* at a concentration of 100 μM.

Keywords: *Xylaria* sp.; pyranone derivative; sesquiterpenoid; antimicrobial activity

Citation: Zhang, Y.; Jin, Y.; Yan, W.; Gu, P.; Zeng, Z.; Li, Z.; Zhang, G.; Wei, M.; Xue, Y. New Pyranone Derivatives and Sesquiterpenoid Isolated from the Endophytic Fungus *Xylaria* sp. Z184. *Molecules* **2024**, *29*, 1728. https://doi.org/10.3390/molecules29081728

Academic Editors: Radosław Kowalski and Tomasz Baj

Received: 18 March 2024
Revised: 3 April 2024
Accepted: 5 April 2024
Published: 11 April 2024

1. Introduction

Natural products (NPs) have always been an indispensable source of new drugs [1]. As an important source of NPs with novel structures and high-value biological activities, plant endophytic fungi have always been attracting broad attention from natural product chemists and pharmacologists [2,3]. Xylariaceae is one of the largest, most commonly encountered, and highly diverse fungal families of the Ascomycota [4]. The genus *Xylaria*, belonging to the family Xylariaceae, is medicinal fungi commonly found in decaying plant tissues and is widely distributed in temperate, tropical, and subtropical regions [5,6]. So far, more than 200 bioactive compounds (>100 new ones) were isolated from *Xylaria*, including cytochalasins, α-pyrones, cyclopeptides, terpenoids, lactones, and succinic acid derivatives [7]. Furthermore, the secondary metabolites produced by species of *Xylaria* have been found to exert a wide range of biological activities, such as anti-inflammatory, antifungal, antibacterial, anti-tumor, and α-glucosidase-inhibitory activities [7,8].

As part of our group's ongoing effort to identify bioactive natural products from medicinal plants and endophytic fungi [9–11], the fungus *Xylaria* sp. Z184, isolated from the leaves of *Fallopia convolvulus* (L.) Á. Löve for the first time, has attracted our attention for

its impressive compound abundance in TLC and HPLC analyses (Figure S106). Our current investigation on this strain led to the isolation of three new pyranone derivatives, called fallopiaxylaresters A–C (**1**–**3**), a new bisabolane-type sesquiterpenoid fallopiaxylarol A (**4**) (Figure 1), and the first complete set of the spectroscopic data for the previously disclosed pestalotiopyrone M (**5**), as well as a suite of known compounds consisting of six pyranone derivatives (**6**–**11**), three sesquiterpenoids (**12**–**14**), three isocoumarin derivatives (**15**–**17**), and one aromatic allenic ether (**18**). Herein, the details of the isolation, structure elucidation of all new compounds and their anti-inflammatory, antimicrobial, and α-glucosidase-inhibitory activities were described.

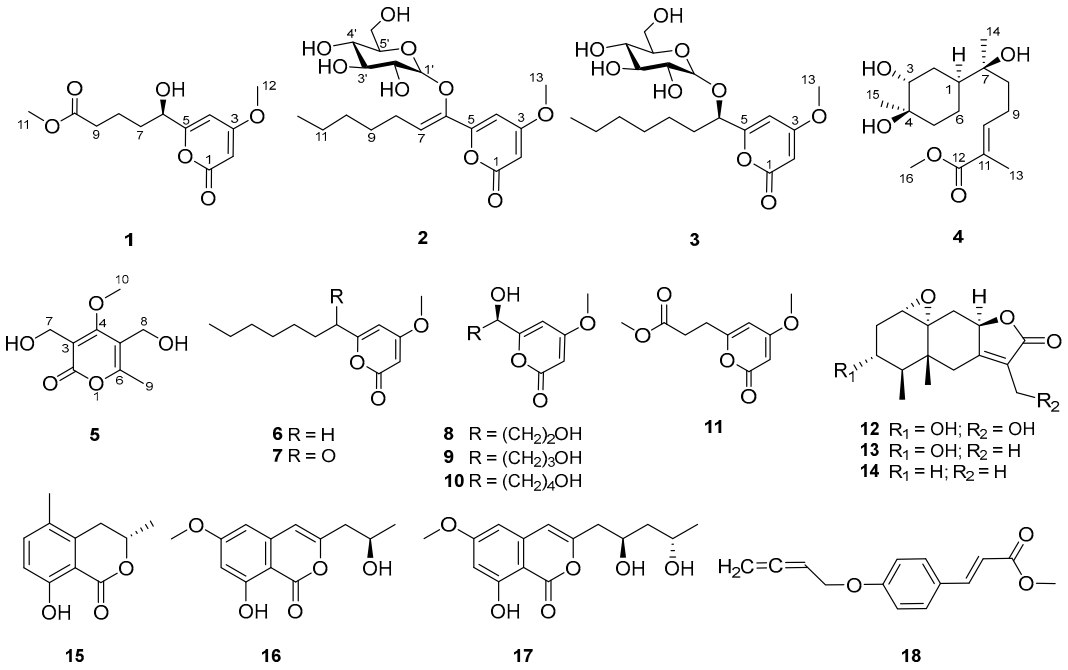

Figure 1. Chemical structures of compounds **1**–**18**.

2. Results and Discussion

Compound **1**, named fallopiaxylarester A, was obtained as a white solid. Its molecular formula $C_{12}H_{16}O_6$ was determined by the HRESIMS molecular ion peak at m/z 279.0837 $[M + Na]^+$ (calcd for $C_{12}H_{16}O_6Na$, 279.0839). The IR absorption bands showed the presence of hydroxyl (3426 cm^{-1}) and carbonyl (1733 cm^{-1}) functionalities. Detailed comparison of ^1H and ^{13}C NMR spectra of **1** and **10** revealed that the structure of **1** is almost identical with that of **10**, which was supported by the further analysis of 2D NMR spectra (Table 1). The HMBC correlations of **1** from H-2 (δ_H 5.56) to C-1/C-3/C-4, from H_3-12 (δ_H 3.87) to C-3, from H-4 (δ_H 6.22) to C-3/C-5/C-6, and from H-6 (δ_H 4.35) to C-5 and C-8, showed the same settlement as with compound **10** (Figure 2). The main difference between **1** and **10** was found at C-10 of the side chain of the pyranone core, replaced by the fragment of methyl valerate group. This deduction was further identified by the HMBC correlations from H_3-11 (δ_H 3.66) and H_2-9 (δ_H 2.38) to C-10. Thus, the planar structure of **1** was established. Since there was only one chiral center in the molecule, the relative configuration was arbitrarily assigned as 6*R**. The absolute configuration of C-6 was subsequently assigned to be *R* by comparing the optical rotational value $[\alpha]_D^{25}$ +56.2 (*c* 0.11, MeOH) with $[\alpha]_D^{25}$ +96.0 (*c* 0.10, MeOH) of compound **10** [12]. Furthermore, the deduction was also confirmed by a time-dependent density functional theory–electronic circular dichroism (TDDFT-ECD) approach. As shown in Figure 3, the Boltzmann-averaged ECD spectrum of (6*R*)-**1** displayed a similar curve compared to the experimental one. Thus, the absolute configuration at C-6 in **1** was unambiguously assigned as 6*R* (Figure 1).

Table 1. ^{1}H NMR (δ_H, 600 MHz) and ^{13}C NMR (δ_C, 150 MHz) data for **1** in methanol-d_4.

No.	δ_H, Mult (*J* Hz)	δ_C, Type
1		167.0, C
2	5.56, d (2.1)	88.6, CH
3		173.8, C
4	6.22, d (2.1)	99.9, CH
5		168.7, C
6	4.35, dd (7.2, 4.8)	70.7, CH
7	1.83, m 1.68, m, overlap	35.2, CH_2
8	1.76, m 1.69, m, overlap	21.7, CH_2
9	2.38, t (6.7)	34.4, CH_2
10		175.6, C
11	3.66, s	52.0, CH_3
12	3.87, s	57.0, CH_3

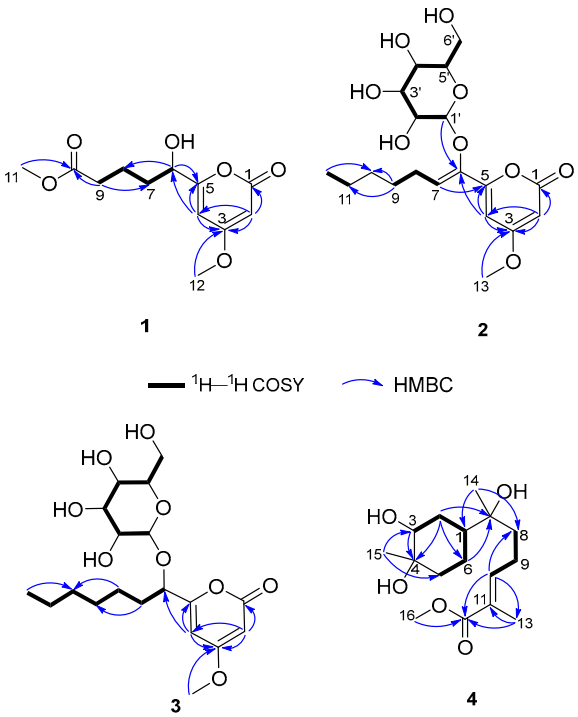

Figure 2. The key ^{1}H–^{1}H COSY and HMBC correlations of **1**–**4**.

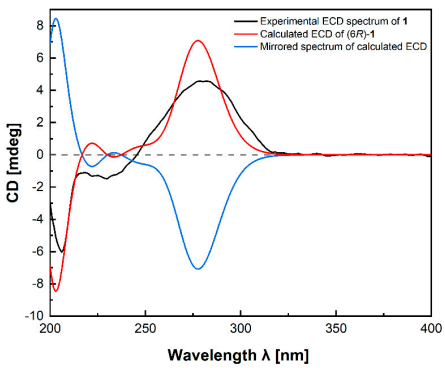

Figure 3. Experimental ECD spectrum of fallopiaxylarester A (**1**) (black); calculated ECD of (6*R*)–**1** (red); mirrored spectrum of calculated ECD (blue).

Compound **2**, a white solid, was determined to possess the molecular formula of $C_{19}H_{28}O_9$ with six degrees of unsaturation by using HRESIMS {*m*/*z* 423.1626 $[M + Na]^+$, (calcd for $C_{19}H_{28}O_9Na$, 423.1626)}. The spectra of **2** showed similar absorption bands, indicating the same presence of hydroxyl (3359 cm^{-1}) and carbonyl (1696 cm^{-1}) functionalities. The ^1H NMR spectra data showed signals of a typical sugar moiety at δ_H 5.12 (d, *J* = 3.7 Hz), 3.53 (dd, *J* = 10.0, 3.7 Hz), 3.78 (t, *J* = 9.3 Hz), 3.45 (t, *J* = 9.3 Hz), 3.90 (m), and 3.76 (m) (Table 2). Analysis of the ^{13}C NMR and DEPT spectra of **2** indicated the presence of 19 carbon signals, assignable to two methyl carbons (one methoxyl, δ_C 57.0 and 14.4), five methylene carbons (δ_C 27.1, 30.0, 32.8, 23.6 and 62.1), eight methine carbons (three olefinic, δ_C 89.4, 100.2, 125.0, 102.8, 73.4, 74.4, 71.0, and 75.5), one ester carbonyl carbon (δ_C 166.7), and three olefinic quaternary carbons (δ_C 174.0, 157.9 and 145.8). These substructures accounted for four out of five degrees of unsaturation, indicating one cyclic system in **2**. The ^1H–^1H COSY spectrum revealed three spin systems: (a) H-7/H-8/H-9; (b) H-11/H-12; and (c) H-1′/H-2′/H-3′/H-4′/H-5′/H-6′ (Figure 2). And those spin systems were connected by the key HMBC correlations from H-2 (δ_H 5.59) to C-1/C-3/C-4, from H_3-13 (δ_H 3.87) to C-3, from H-4 (δ_H 6.95) to C-3/C-5/C-6, from H-7 (δ_H 6.07) to C-5, and from H_2-9 (δ_H 1.48) to C-10/C-11.

Table 2. ^1H NMR (δ_H, 600 MHz) and ^{13}C NMR (δ_C, 150 MHz) data for **2**.

No.	δ_H, Mult (*J* Hz) [a]	δ_C, Type [a]	δ_H, Mult (*J* Hz) [b]	δ_C, Type [b]	δ_H, Mult (*J* Hz) [c]	δ_C, Type [c]
1		166.7, C		164.1, C		162.7, C
2	5.59, d (2.2)	89.4, CH	5.70, d (2.2)	89.7, CH	5.61, d (2.2)	88.6, CH
3		174.0, C		172.3, C		171.2, C
4	6.95, d (2.2)	100.2, CH	7.64, d (2.2)	99.7, CH	6.98, d (2.2)	98.3, CH
5		157.9, C		157.5 C		155.8, C
6		145.8, C		146.1, CH		144.3, C
7	6.07, t (7.5)	125.0, CH	6.24, t (7.5)	123.6, CH	5.91, t (7.5)	122.8, CH
8	2.42, m	27.1, CH_2	2.61, q (7.5)	26.9, CH_2	2.33, dd (15.0, 7.6)	25.3, CH_2
9	1.48, m	30.0, CH_2	1.33, m	29.7, CH_2	1.39, m	28.4, CH_2
10	1.36, m, overlap	32.8, CH_2	1.19, m, overlap	32.3, CH_2	1.28, m, overlap	31.1, CH_2
11	1.37, m, overlap	23.6, CH_2	1.18, m, overlap	23.2, CH_2	1.29, m, overlap	22.0, CH_2
12	0.92, t (6.9)	14.4, CH_3	0.75, t (7.0)	14.6, CH_3	0.87, t (6.9)	13.9, CH_3
13	3.87, s	57.0, CH_3	3.60, s	56.5, CH_3	3.81, s	56.4, CH_3
1′	5.12, d (3.7)	102.8, CH	5.68, d (3.7)	103.4, CH	4.96, d (3.7)	101.3, CH
2′	3.53, dd (10.0, 3.7)	73.4, CH	4.27, dd (10.5, 4.1)	74.0, CH	3.32, m, overlap	71.7, CH
3′	3.78, t (9.3)	74.4, CH	4.71, t (9.3)	75.2, CH	3.70, m	72.5, CH
4′	3.45, t (9.3)	71.0, CH	4.35, t (10.0)	71.9, CH	3.22, m	69.4, CH
5′	3.90, m	75.5, CH	4.66, dt (10.0, 3.5)	76.8, CH	3.54, m, overlap	74.7, CH
6′	3.76, m	62.1, CH_2	4.48, br s	62.9, CH_2	3.55, m, overlap	60.3, CH_2
2′-OH					5.52, d (4.9)	
3′-OH					5.10, m	
4′-OH					5.10, m	
6′-OH					4.53, t (5.8)	

[a] Measured in methanol-d_4, [b] measured in pyridine-d_5, [c] measured in DMSO-d_6.

Subsequently, the long-range HMBC correlation from H-1′ (δ_H 5.12) to the anomeric carbon C-6 suggested the sugar was attached at the C-6 of the side chain. Acid hydrolysis of **2** followed by HPLC analysis of the sugar derivative was applied to determine the type of sugar moiety, but without success. Then, a different deuterated solvent, pyridine-d_5, was used to analyze the proton signals on the sugar. In addition, the isolated anomeric proton signal was probed by a selective 1D-TOCSY experiment. In the 1D-TOCSY experiment, irradiation of the signal at δ_H 5.68 (1H, d, *J* = 3.7 Hz) enabled the identification of H-2′ (δ_H 4.27, dd, *J* = 10.5, 4.1 Hz), H-3′ (δ_H 4.71, t, *J* = 9.3 Hz), H-4′ (δ_H 4.35, t, *J* = 10.0 Hz), H-5′ (δ_H 4.66, dt, *J* = 10.0, 3.5 Hz), and H_2-6′ (δ_H 4.48, br s) in the same conjugated system (Figure 4, Table 2). The *J* values of $J_{H\text{-}5'/H\text{-}4'}$ (10.0 Hz) and $J_{H\text{-}5'/H\text{-}6'}$ (3.5 Hz) in ^1H NMR

in pyridine-d_5 of **2** combined with the 1D-TOCSY experiment suggested an α-D-glucose. Furthermore, those chemical shift values of anomeric carbon at δ_C 102.8 (C-1′), four tertiary carbons at δ_C 73.4 (C-2′), 74.4 (C-3′), 71.0 (C-4′), 75.5 (C-5′), and a methylene oxide carbon at δ_C 62.1 (C-6′) in methanol-d_4 were highly similar to 6-Buty-AA-2G along with other derivatives of AA-2G in the literature [13], which also confirmed the inference that the sugar unit was α-D-glucose. In addition, the geometry of the double bond between C-6 and C-7 was inferred by the ROESY spectrum in DMSO-d_6. The ROESY correlations between H_2-8 (δ_H 2.33) and H-1′ (δ_H 4.96)/H-3′ (δ_H 3.70)/H-5′ (δ_H 3.54), and between H-4 (δ_H 6.98) and H-1′/H-3′, demonstrated the *Z* geometry of $\Delta^{6,7}$ (Figures 5 and S15). Thus, this undescribed **2** was established as shown in Figure 1 and named fallopiaxylarester B.

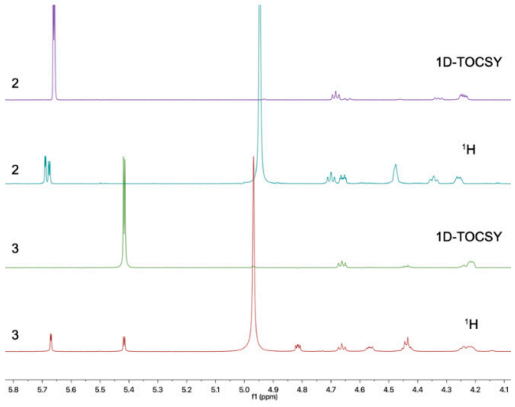

Figure 4. 1D-TOCSY spectra of compounds **2** (purple) and **3** (green).

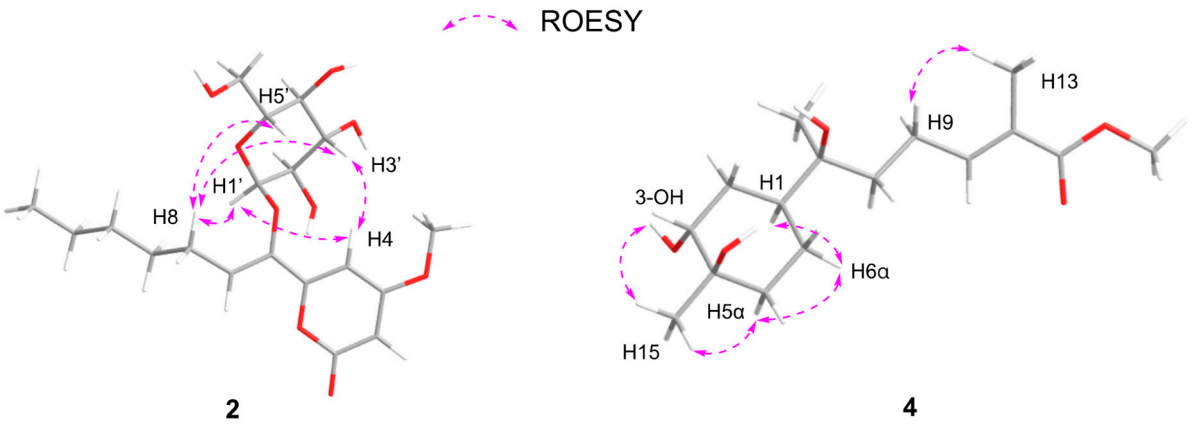

Figure 5. Energy-minimized structures of **2** and **4** with the key ROESY correlations.

Compound **3**, named fallopiaxylarester C, was isolated as a white solid. Its molecular formula of $C_{19}H_{30}O_9$ with five degrees of unsaturation was based on HRESIMS analysis {*m*/*z* 425.1780 $[M + Na]^+$, (calcd for $C_{19}H_{30}O_9Na$, 425.1782)}. Like **2**, the presence of α, β-unsaturated γ-lactone and hydroxyl groups in **3** was obvious by its IR absorption bands at υ_{max} 3380 and 1700 cm^{-1}. Furthermore, with the analysis of 1D NMR spectra, a sugar moiety in **3** was also quickly recognized. In addition, the HMBC correlation from H-6 (δ_H 4.52) to C-1′ suggested the same set as with **2** (Table 3). The main difference between these two compounds was the hydrogenation of the trisubstituted olefinic group at C-6/C-7 in **2**, with a 2 mass unit difference between **2** and **3**. Subsequently, an acid hydrolysis of **3** afforded the products, including a pyrone aglycone **3a** and a sugar moiety **3b**. The absolute configuration of C-6 in **3a** was assigned to be *R* form by comparing its optical value $[\alpha]_D^{25}$ +52.5 (*c* 0.11, MeOH) with +67.6 (*c* 0.25, MeOH) of nodulisporipyrones A [14]. According to the detailed analysis of ^1H NMR and 1D-TOCSY experiment of **3**, H-1′ (δ_H 5.42, d, *J* = 3.8Hz), H-2′ (δ_H 4.22, dd, *J* = 9.6, 3.8 Hz), H-3′ (δ_H 4.67, t, *J* = 9.6 Hz), H-4′

(δ_H 4.24, t, J = 9.6 Hz), H-5′ (δ_H 4.44, t, J = 9.6 Hz), H_2-6′ (δ_H 4.57, dd, J = 9.6, 5.6 Hz; δ_H 4.43, m), the sugar moiety was indicated as α-D-glucose (Figure 4, Table 3). Moreover, large similarities were observed by comparison of NMR data in DMSO-d_6 of **3** with 5-(α-D-glucopyranosyloxymethyl)-2-furancarboxylic acid and other analogs in the literature [15]. Thus, the structure of **3** was established as shown (Figure 1).

Table 3. ^{1}H NMR (δ_H, 600 MHz) and ^{13}C NMR (δ_C, 150 MHz) data for **3**.

No.	δ_H, Mult (J Hz) [a]	δ_C, Type [a]	δ_H, Mult (J Hz) [b]	δ_C, Type [b]	δ_H, Mult (J Hz) [c]	δ_C, Type [c]
1		167.1, C		164.5, C		164.2, C
2	5.57, d (2.2)	89.1, CH	5.68, d (2.3)	89.1, CH	5.57, d (2.2)	88.0, CH
3		173.6, C		171.9, C		170.9, C
4	6.55, d (2.2)	101.9, CH	6.99, d (2.3)	100.5, CH	6.50, d (2.2)	99.4, CH
5		165.5, C		165.8, C		163.3, C
6	4.52, t (6.2)	75.3, CH	4.82, dd (7.8, 4.4)	74.8, CH	4.38, dd (6.8, 4.8)	72.9, CH
7	1.85, dd (14.0, 7.6)	35.1, CH_2	1.89, m 1.84, m	35.2, CH_2	1.70, m	33.5, CH_2
8	1.43, m	26.2, CH_2	1.51, m	26.2, CH_2	1.32, m	24.4, CH_2
9	1.35, m 1.33, m	30.1, CH_2	1.18, m, overlap 1.10, m, overlap	29.7, CH_2	1.27, m, overlap	28.4, CH_2
10	1.31, m, overlap	32.8, CH_2	1.08, m, overlap	32.2, CH_2	1.23, m, overlap	31.1, CH_2
11	1.32, m, overlap	23.7, CH_2	1.16, m, overlap	23.3, CH_2	1.25, m, overlap	22.0, CH_2
12	0.90, t (6.8)	14.4, CH_3	0.78, t (7.3)	14.7, CH_3	0.85, t (6.8)	14.0, CH_3
13	3.87, s	57.0, CH_3	3.63, s	56.4, CH_3	3.81, s	56.4, CH_3
1′	4.80, d (3.8)	98.5, CH	5.42, d (3.8)	99.3, CH	4.66, d (3.8)	97.2, CH
2′	3.41, dd (9.8, 3.8)	73.2, CH	4.22, dd (9.6, 3.8)	74.0, CH	3.22, m	71.5, CH
3′	3.68, m, overlap	74.8, CH	4.67, t (9.6)	75.6, CH	3.45, m, overlap	73.7, CH
4′	3.29, m	71.7, CH	4.24, t (9.6)	72.6, CH	3.07, m	70.1, CH
5′	3.68, m, overlap	74.6, CH	4.44, t (9.6)	75.8, CH	3.45, m, overlap	73.0, CH
6′	3.68, m, overlap 3.83, m	62.7, CH_2	4.57, dd (9.6, 5.6) 4.43, m	63.3, CH_2	3.61, m 3.45, m, overlap	60.9, CH_2
2′-OH					5.04, d (5.9)	
3′-OH					4.92, d (4.1)	
4′-OH					4.99, d (5.2)	
6′-OH					4.52, t (5.4)	

[a] Measured in methanol-d_4, [b] measured in pyridine-d_5, [c] measured in DMSO-d_6.

Compound **4** was isolated as a colorless oil. Its molecular formula of $C_{16}H_{28}O_5$ with three degrees of unsaturation was also based on HRESIMS analysis {m/z 323.1829 $[M + Na]^+$, (calcd for $C_{16}H_{28}O_5Na$, 323.1829)}. The IR spectrum of **4** demonstrated characteristic absorption bands for hydroxyl (3425 cm^{-1}) and carbonyl (1687 cm^{-1}) groups. The 1D NMR and HSQC spectra of **4** revealed 16 carbon signals, including four methyl groups, five sp^3 methylene groups, one sp^2 methine, two sp^3 methine groups, and four quaternary carbons (three oxygenated carbons) (Table 4). The above information accounted for two degrees of unsaturation, indicating one cyclic system in compound**4**. The ^{1}H–^{1}H COSY spectrum revealed two spin systems: (a) H-5/H-6/H-1/H-2/H-3, and (b) H-8/H-9/H-10 (Figure 2). Furthermore, the HMBC correlations from H_3-15 (δ_H 1.04) to C-3/C-5, from H_2-2 (δ_H 1.59, 1.53)/H-3 (δ_H 3.36) to C-4, from H_2-2 (δ_H 1.59, 1.53)/H_2-6 (δ_H 1.29) to C-7, from H_3-14 (δ_H 0.96) to C-1/C-8, from H-10 (δ_H 6.71) to C-8/C-12/C-13, from H_3-13 (δ_H 1.77) to C-11/C-12, and from H_3-16 (δ_H 3.64) to C-12 made those two spin systems connected. Thus, the planar structure of **4** was established as shown (Figure 1) and named fallopiaxylarol A.

Table 4. ^{1}H NMR (δ_H, 600 MHz) and ^{13}C NMR (δ_C, 150 MHz) data for **4**.

No.	δ_H, Mult (*J* Hz) [a]	δ_C, Type [a]	δ_H, Mult (*J* Hz) [b]	δ_C, Type [b]
1	1.72, m	39.1, CH	1.59, m, overlap	38.8, CH
2	1.80, m	29.3, CH_2	1.59, m, overlap 1.53 m	29.2, CH_2
3	3.66, br s	74.0, CH	3.36, m, overlap	72.6, CH
4		70.9, C		69.5, C
5	1.74, m 1.55, m	33.6, CH_2	1.49, m 1.29, m, overlap	33.5, CH_2
6	1.49, m 1.40, m	22.1, CH_2	1.29, m, overlap	21.7, CH_2
7		74.0, C		72.0, C
8	1.60, m	38.8, CH_2	1.41, m	38.1, CH_2
9	2.26, m	22.9, CH_2	2.18, q (8.0)	22.7, CH_2
10	6.77, td (7.5, 1.2)	142.6, CH	6.71, td (7.5, 0.9)	143.5, CH
11		127.6, C		126.4, C
12		168.8, C	0.90, t (6.8)	167.7, C
13	1.84, s	12.4, CH_3	1.77, s	12.2, CH_3
14	1.14, s	23.7, CH_3	0.96, s	23.8, CH_3
15	1.26, s	27.6, CH_3	1.04, s	27.9, CH_3
16	3.73, s	51.8, CH_3	3.64, s	51.6, CH_3
3-OH			4.36, d (4.0)	
4-OH			3.96, s	
7-OH			3.88, s	

[a] Measured in chloroform-*d*, [b] measured in DMSO-d_6.

Initially, the ROESY correlation between H_3-13 and H_2-9 and the lack of correlation of H_3-13/H-10 assigned the *E*-geometry of $\Delta^{10, 11}$, which was also supported by the *J* value of H-10 (7.5) (Figure 5). In addition, the ROESY correlations of H-1/3-OH/H_3-15/H-5α/H-6α suggested the *cis* orientation of the H-1, 3-OH, and H_3-15. Furthermore, the literature survey revealed that the NMR data of the six-membered ring and the optical rotation values of **4** were almost identical to those of (1*S*,3*R*,4*R*,7*S*)-3,4-dihydroxy-α-bisabolol [16]. Thus, the absolute configuration of **4** was tentatively determined as shown in Figure 1.

After the literature survey, as for the secondary metabolites produced by the genus *Xylaria*, the main structural differences between the co-isolated new pyranone derivatives in this case and the other analogues of the genus are the variation of substituents in the side chain attached pyranone core [7,12,16]. Although compound **5** has previously been reported as a natural product from fermentation extracts of endophytic fungi [17], this is the first report of its existence to be accompanied by a full suite of supporting spectroscopic data. The 14 known compounds, pestalotiopyrone M (**5**), 4-methoxy-6-nonyl-2-pyrone (**6**) [18], xylariaopyrone A (**7**) [19], xylariaopyrone H (**8**) [12], xylariaopyrone I (**9**) [12], xylapyrone D (**10**) [20], scirpyrone H (**11**) [21], 1α,10α-epoxy-3α,13-dihydroxyeremophil-7(11)-en-12,8β-olide (**12**) [4], 3α-hydroxymairetolide A (**13**) [4], mairetolide A (**14**) [22], (−)-5-methylmellein (**15**) [23], diaporthin (**16**) [24], mucorisocoumarin B (**17**) [25], and eucalyptene (**18**) [26], were also isolated from *Xylaria* sp. Z184. The structures of these compounds (**5**–**18**) were identified by comparing the spectral data to those reported in the respective references (Figures S80–S105).

The secondary metabolites generated by stains of *Xylaria* usually show obvious anti-inflammatory and antifungal activities [7,8]. In this case, compounds **2**–**10** and **15**–**18** and the crude extract were selected to evaluate the antimicrobial, anti-inflammatory and α-glucosidase-inhibition activities due to the limitation of samples. In antimicrobial assay, compounds **5**, **7**, and **8** displayed weak activity against *Staphylococcus areus* subsp. *aureus* with inhibition ratios of 25.9%, 31.5%, and 25.3% at a concentration of 100 μM. Unfortunately, in anti-inflammatory and α-glucosidase assay, only the crude extract potently inhibited LPS-induced NO production in RAW264.7 mouse macrophages, with an inhibition rate of 77.28 ± 0.82% at a concentration of 50 μg/mL. Although it was cytotoxic at

this concentration, reducing the concentration to 6.25 μg/mL abrogated the cytotoxicity (Table 5).

Table 5. Inhibitory activities of compounds selected and crude extract on LPS-stimulated NO production.

Compounds	Concentration	NO Production Inhibition (%) [a]
2	50 μM	4.51 ± 0.35
3	50 μM	–3.93 ± 2.43
4	50 μM	1.85 ± 3.18
5	50 μM	–1.61 ± 0.53
12	50 μM	0.92 ± 2.97
13	50 μM	4.67 ± 2.36
14	50 μM	3.54 ± 1.26
18	50 μM	–0.92 ± 2.21
Crude extract	50 μg/mL	77.28 ± 0.82
	6.25 μg/mL	7.78 ± 3.29
L-NMMA [b]	50 μM	53.75 ± 1.28

[a] All compounds examined in a set of triplicated experiment. [b] Positive control.

3. Materials and Methods

3.1. General Experimental Procedures

Optical rotations were determined with a PerkinElmer 341 polarimeter (PerkinElmer, Waltham, MA, USA). UV absorptions were obtained by using a Waters UV-2401A spectrophotometer equipped with a DAD and a 1 cm path length cell. Methanolic samples were scanned from 190 to 400 nm in 1 nm steps. Measurements of IR spectra were performed using a Bruker Vertex 70 FT-IR spectrometer (Bruker, Karlsruhe, Germany). NMR spectra were recorded on Bruker AM-400 and AM-600 NMR spectrometers (Bruker, Karlsruhe, Germany) with TMS as internal standard, and NMR data were referenced to selected chemical shifts of methanol-d_4 (^{1}H: 3.31 ppm, ^{13}C: 49.0 ppm), chloroform-*d* (^{1}H: 7.26 ppm, ^{13}C: 77.0 ppm), and dimethyl sulfoxide-d_6 (^{1}H: 2.50 ppm, ^{13}C: 39.5 ppm), respectively. HRESIMS data were acquired on a Thermo Fisher LTQ XL LC/MS (Thermo Fisher, Palo Alto, CA, USA). Semi-preparative HPLC was performed on an Agilent 1220 instrument equipped with a UV detector with a semi-preparative column (RP-C_{18}, 5 μm, 250 × 10 mm, Welch Materials, Inc., Shanghai, China). Column chromatography was performed using Sephadex^{TM} LH-20 gel (40–70 μm; Merck KGaA, Darmstadt, Germany), and precoated silica gel plates (GF254, Qingdao Marine Chemical Co., Ltd., Qingdao, China) were used for TLC analyses. Spots were visualized by heating silica gel plates sprayed with 10% H_2SO_4 in EtOH. All HPLC solvents were purchased from Guangdong Guanghua Sci-Tech Co., Ltd. (Guangzhou, China). All solvents were of analytical grade (Guangzhou Chemical Regents Company, Ltd., Guangzhou, China).

3.2. Fungal Material

The fungus *Xylaria* sp. Z184 was isolated from the leaves of *Fallopia convolvulus* (L.) Á. Löve collected in Zhuyang Town, Henan province, P. R. China (N 34°14′12″ W 110°47′09″) in June 2022. Leaves of *F. convolvulus* (L.) Á. Löve were processed within 24 h and rinsed with sterile water. On a sterile workbench, after 30 min of ultraviolet light exposure, the leaves underwent sequential treatment with a 5% sodium hypochlorite solution, sterile water, and 75% ethanol, either soaked or rinsed, followed by drying with sterile filter paper. Leaves were trimmed into small squares with sterile scissors and placed into previously prepared PDA monoclonal agar plates, inoculating three petri plates in parallel. These plates were incubated at 30 °C for 3–7 days, until mycelial growth was observed extending from the inside of the tissue block to its surroundings. Distinct morphological colonies were subsequently transferred to new media for continued cultivation. This procedure

was repeated until the fungal strains showed uniform growth, leading to the isolation of purified strains (Figure 6).

Figure 6. Photo of the fungus *Xylaria* sp. Z184.

To identify the strains, the standardized operating procedure was performed, which included genomic DNA extraction, 16*S*/18*S* amplification, PCR product detection and purification, and comparison of sequencing results with the NCBI-BLAST database (https://www.ncbi.nlm.nih.gov/) accessed on 10 December 2022, using ITS1 and ITS4 primers for both amplification and sequencing. The sequence data for this strain was submitted to the GenBank under accession No. KU645984. The fungal strain was deposited on 20% aqueous glycerol stock in a −80 °C freezer at the School of Pharmaceutical Sciences (Shenzhen), Shenzhen Campus of Sun Yat-sen University, Shenzhen, China.

3.3. Fermentation, Extraction, and Isolation

Xylaria sp. Z184 was cultured on potato dextrose agar for 5 days at 28 °C to prepare the seed culture. The cultured agar plates were cut into small pieces, which were then inoculated into 30 previously autoclaved Erlenmeyer flasks (350 mL), each containing 50 g of rice and 45 mL of distilled water. All flasks were incubated at 28 °C for 40 days. Cultural media was extracted with methanol four times, and the solvent was evaporated under reduced pressure at 45 °C. Then the extract was suspended in water and extracted four times with ethyl acetate. The combined ethyl acetate layers were concentrated under reduced pressure to yield a brown extract (7.5 g).

The crude extract was chromatographed on Sephadex LH-20 (MeOH) to give eight fractions (Fr.1–Fr.8). Fr. 3 (2.8 g) was separated with silica gel column chromatography (CC) with petroleum ether (PE)/EtOAc (20:1–0:1, *v*/*v*) to give seven subfractions (Fr. 3.1–Fr. 3.7). Fr. 3.3 (306.2 mg) was purified with silica gel CC using PE/EtOAc (15:1–1:1, *v*/*v*) to yield six further subfractions (Fr. 3.3.1–Fr. 3.3.6). Fr. 3.3.4 (25.8 mg) was purified by semi-preparative HPLC (MeOH/H_2O, 48:52, *v*/*v*, 3.0 mL/min) to yield compound **7** (4.3 mg, t_R 22.0 min). Fr. 4 (1.7 g) was separated by silica gel CC with CH_2Cl_2/MeOH (80:1–0:1, *v*/*v*) to obtain seven subfractions (Fr. 4.1–Fr. 4.7). Fr. 4.3 (277.5 mg) was purified by semi-preparative HPLC (MeCN/H_2O, 25:75, 0–14 min, then MeCN/H_2O, 50:50, 14.01–33 min, *v*/*v*, 3.0 mL/min) to yield compounds **13** (4.6 mg, t_R 12.1 min), **14** (1.6 mg, t_R 27.6 min), and **6** (4.1 mg, t_R 31.5 min). Fr. 4.5 (239.9 mg) was purified by semi-preparative HPLC (MeCN/H_2O, 20:80, 0–10 min, then MeCN/H_2O, 40:60, 10.01–21 min, *v*/*v*, 3.0 mL/min) to yield compounds **10** (8.7 mg, t_R 13.2 min) and **4** (6.0 mg, t_R 19.5 min). Fr. 4.6 (225.9 mg) was purified by semi-preparative HPLC (MeOH/H_2O, 40:60, *v*/*v*, 3.0 mL/min) to yield compounds **2** (3.9 mg, t_R 30.1 min) and **3** (12.1 mg, t_R 35.5 min). Fr. 5 (1.3 g) was separated with silica gel CC with CH_2Cl_2/MeOH (25:1–0:1, *v*/*v*) to give six subfractions (Fr. 5.1—Fr. 5.6). Fr. 5.1 (44.0 mg) was further purified by semi-preparative HPLC (MeOH/H_2O, 55:45, 0–23 min, then MeOH/H_2O, 65:35, 23.01–47 min, *v*/*v*, 3.0 mL/min) to yield compounds **15** (3.1 mg, t_R 21.8 min) and **18** (1.4 mg, t_R 45.5 min). Fr. 5.3 (399.7 mg) was purified by semi-preparative HPLC (MeOH/H_2O, 35:65, 0–19 min, then MeOH/H_2O, 54:46, 19.01–40 min, *v*/*v*, 3.0 mL/min) to yield compounds **1** (1.2 mg, t_R 6.0 min), **17** (8.3 mg, t_R 18.1 min), **16** (2.7 mg, t_R 31.9 min), and **11** (2.4 mg, t_R 38.2 min). Similarly, Fr. 5.4 (355.8 mg) was purified

by semi-preparative HPLC (MeCN/H_2O, 10:90, *v*/*v*, 3.0 mL/min) to yield compounds **5** (3.5 mg, t_R 6.5 min), **8** (1.3 mg, t_R 8.1 min), **9** (8.3 mg, t_R 10.9 min), and **12** (2.1 mg, t_R 15.5 min).

3.4. Spectral and Physical Data of Compounds **1**–**5**

Fallopiaxylarester A (**1**): White solid; $[\alpha]_D^{25}$ +56.2 (*c* 0.11, MeOH); UV (MeOH) λ_{max} (log ε): 279 (0.19), 204 (0.72) nm; IR (KBr) υ_{max}: 3426, 2922, 1733, 1648, 1569, 1457, 1412, 1384, 1247, 1032, 832 cm^{-1}; ECD (MeOH) λ_{max} ($\Delta\varepsilon$): 279 (+3.0), 206 (–4.0) nm. ^1H and ^{13}C NMR data, see Table 1; HRESIMS (*m*/*z*): 279.0837 $[M + Na]^+$ (calcd for $C_{12}H_{16}O_6Na$, 279.0839).

Fallopiaxylarester B (**2**): White solid; $[\alpha]_D^{25}$ +102.9 (*c* 0.38, MeOH); UV (MeOH) λ_{max} (log ε): 310 (0.16), 260 (0.06), 219 (0.41) nm; IR (KBr) υ_{max}: 3359, 2928, 2858, 1696, 1623, 1560, 1456, 1409, 1260, 1230, 1080, 1018, 817, 539 cm^{-1}; ECD (MeOH) λ_{max} ($\Delta\varepsilon$): 310 (+3.4), 231 (–4.1), 205 (–3.3) nm. ^1H and ^{13}C NMR data, see Table 2; HRESIMS (*m*/*z*): 423.1626 $[M + Na]^+$ (calcd for $C_{19}H_{28}O_9Na$, 423.1626).

Fallopiaxylarester C (**3**): White solid; $[\alpha]_D^{25}$ +124.2 (*c* 0.39, MeOH); UV (MeOH) λ_{max} (log ε): 281 (0.11), 204 (0.45) nm; IR (KBr) υ_{max}: 3380, 2927, 2857, 1700, 1649, 1569, 1458, 1414, 1384, 1250, 1025, 836, 700 cm^{-1}; ECD (MeOH) λ_{max} ($\Delta\varepsilon$): 280 (+4.5), 232 (+0.9), 205 (+3.0) nm; ^1H and ^{13}C NMR data, see Table 3; HRESIMS (*m*/*z*): 425.1780 $[M + Na]^+$ (calcd for $C_{19}H_{30}O_9Na$, 425.1782).

Fallopiaxylarol A (**4**): Colorless oil; $[\alpha]_D^{25}$ –31.8 (*c* 0.10, MeOH); UV (MeOH) λ_{max} (log ε): 205 (0.36), 218 (0.48) nm; IR (KBr) υ_{max}: 3546, 3426, 2945, 2930, 1688, 1287, 1150, 1036 cm^{-1}; ^1H and ^{13}C NMR data, see Table 4; HRESIMS (*m*/*z*): 323.1829 $[M + Na]^+$ (calcd for $C_{16}H_{28}O_5Na$, 323.1829).

Pestalotiopyrone M (**5**): White solid; UV (MeOH) λ_{max} nm (log ε) 206 (0.45), 293 (0.16); IR (KBr) ν_{max} 3311, 2961, 2928, 1711, 1565, 1365, 1014, 989 cm^{-1}; ^1H NMR (methanol-d_4, 600 MHz) δ_H: 4.54 (2H, s, H-7), 4.41 (2H, s, H-8), 4.18 (3H, s, H-10), 2.35 (3H, s, H-9); ^{13}C NMR (methanol-d_4, 150 MHz) δ_C: 171.6 (C, C-4), 167.4 (C, C-2), 163.0 (C, C-6), 115.2 (C, C-5), 110.1 (C, C-3), 63.1 (CH_3, C-10), 55.5 (CH_2, C-8), 55.1 (CH_2, C-7), 17.3 (CH_3, C-9); HRESIMS (*m*/*z*): 223.0578 $[M + Na]^+$ (calcd for $C_9H_{12}O_5Na$, 223.0577).

3.5. Computational Details (TDDFT-ECD) of **1**

The conformational search of (6*R*)-**1** was performed by using torsional sampling (MCMM) conformational searches with an OPLS_2005 force field within an energy window of 21 kJ/mol. Conformers above 1% Boltzmann populations were re-optimized at the B3LYP/6-31G(d) level with the IEFPCM solvent model for methanol. The following TDDFT calculations of the re-optimized geometries were all performed at the B3LYP/6-311G(d,p) level with the IEFPCM solvent model for methanol. Frequency analysis was performed as well to confirm that the re-optimized geometries were at the energy minima. Finally, the SpecDis 1.62 [27] software was used to obtain the Boltzmann-averaged ECD spectra of **1** and visualize the result.

3.6. Biological Assays

3.6.1. Antimicrobial Activity

Compounds **2**–**10** and **15**–**18**, and the crude extract were evaluated for antimicrobial activities against *Staphylococcus aureus* subsp. *aureus* and fluconazole-resistant *Candida albicans*. The antimicrobial assay was conducted according to a previously described method [28]. Samples were added into a 96-well culture plate with a maximum test compound concentration of 100 μM. Bacterial liquid was added to each well until the final concentration was 5×10^5 CFU/mL. The plate was then incubated at 37 °C for 24 h, and the OD values at 595 nm were measured using a microplate reader. Blank bacterial medium served as control.

3.6.2. Anti-Inflammatory Activity

The RAW 264.7 cells (2×10^5 cells/well) were incubated in 96-well culture plates with or without 1 μg/mL lipopolysaccharide (LPS, Sigma Chemical Co., St. Louis, MO, USA) for 24 h in the presence or absence of the test compounds. Supernatant aliquots (50 μL) were then treated with 100 μL Griess reagent (Sigma Chemical Co., St. Louis, MO, USA). The absorbance was measured at 570 nm by using a Synergy TMHT microplate reader (BioTek Instruments Inc., Winooski, VT, USA). In this study, N^G-methyl-L-arginine acetate (L-NMMA, Sigma Chemical Co., USA) was used as a positive control. In the remaining medium, an MTT assay was carried out to determine whether the suppressive effect was related to cell viability. The inhibitory rate of nitric oxide (NO) production = (NO level of blank control − NO level of test samples)/NO level of blank control. The percentage of NO production was evaluated by measuring the amount of nitrite concentration in the supernatants with Griess reagent, as described previously [29].

3.6.3. Alpha-Glucosidase-Inhibition Activity

The α-glucosidase inhibition was assessed according to the slightly modified method of Ma et al. [30]. All samples were dissolved in DMSO at a concentration of 50 μM. The α-glucosidase (Sigma Chemical Co., St. Louis, MO, USA) and substrate (4–Nitrophenyl α-D-glucopyranoside, PNPG, Sigma Chemical Co., St. Louis, MO, USA) were dissolved in potassium phosphate buffer (0.1 M, pH 6.7). The samples were preincubated with α-glucosidase at 37 °C for 10 min. Then, PNPG was quickly added to the 96-well enzyme label plate to start the reaction, and the plate was incubated at 37 °C for 50 min. At the same time, a blank control without samples and a positive control of quercetin (10 mM) was set up. All samples were thoroughly mixed and analyzed in triplicate. The OD value was measured at 405 nm using a microplate reader. The inhibition percentage (%) was calculated by the following equation: Inhibition (%) = $(1 - OD_{\text{sample}})/OD_{\text{control blank}} \times 100$.

4. Conclusions

In this paper, three new pyranone derivatives (**1**–**3**) and a new bisabolane-type sesquiterpenoid (**4**) were discovered from the fungus *Xylaria* sp. Z184. Moreover, we co-isolated 14 previously reported compounds (**5**–**18**), and reported the first complete set of spectroscopic data for pyranone **5**. In vitro bioassays were performed on a number of the isolated compounds and crude fungal extract. Compounds **5**, **7**, and **8** were demonstrated to be weak growth inhibitors of *Staphylococcus aureus* subsp. *Aureus*, and the extract was shown to be a potent inhibitor of NO production in LPS-stimulated RAW 264.7 mouse macrophages, with an inhibition rate of 77.28 ± 0.82% at 50 μg/mL. Although the crude fungal extract showed certain inhibitory activity of NO production in LPS-stimulated RAW 264.7 mouse macrophages, unfortunately, in the subsequent isolated compounds, no such convenient activity was found. This suggests that there may still be other structural types of compounds in the extract that exhibit anti-inflammatory activity. Thus, in addition to revealing four novel compounds, this work enhances understanding of the structural diversity within the *Xylaria* metabolomes.

Supplementary Materials: The following supporting information can be downloaded at: https://www.mdpi.com/article/10.3390/molecules29081728/s1, Figures S1–S79: 1D, 2D NMR spectra, and HRESIMS of compounds **1**–**5**; Figures S80-S105: ^1H and ^{13}C NMR spectra of compounds **6**–**18**; Figure S106: The TLC and HPLC profiles of the crude extract of fungus *Xylaria* sp. Z184.

Author Contributions: Y.Z. led on the isolation and data curation. Y.J. conducted the writing of original draft. W.Y. was responsible for fungal isolation, fermentation, and identification of the samples. P.G. and Z.Z. supported on data curation and analysis. Z.L., G.Z., and M.W. contributed to the evaluation of antimicrobial activity. Y.X. led on funding acquisition and project administration. All authors have read and agreed to the published version of the manuscript.

Funding: This work was financially supported by the National Natural Science Foundation of China (No. 21977120 and 32270296), and the Key Basic Research Program of the Science, Technology, and Innovation Commission of Shenzhen Municipality (JCYJ20200109142215045).

Institutional Review Board Statement: Not applicable.

Informed Consent Statement: Not applicable.

Data Availability Statement: The authors declare that all relevant data supporting the results of this study are available within in the article and its Supplementary Materials file.

Acknowledgments: The authors thank Xiaonian Li, Jianchao Chen, and the Shenzhen Bay Laboratory for their helpful assistance in NMR measurement. And we express our sincere thanks to Kunming Institute of Botany, Chinese Academy of Sciences for providing support in quantum chemical calculation.

Conflicts of Interest: The authors declare no conflicts of interest.

References

1. Newman, D.J.; Cragg, G.M. Natural products as sources of new drugs over the nearly four decades from 01/1981 to 09/2019. *J. Nat. Prod.* **2020**, *83*, 770–803. [CrossRef] [PubMed]
2. Liu, H.; Tan, H.; Chen, Y.; Guo, X.; Wang, W.; Guo, H.; Liu, Z.; Zhang, W. Cytorhizins A-D, four highly structure-combined benzophenones from the endophytic fungus *Cytospora rhizophorae*. *Org. Lett.* **2019**, *21*, 1063–1067. [CrossRef] [PubMed]
3. Han, W.B.; Wang, G.Y.; Tang, J.J.; Wang, W.J.; Liu, H.; Gil, R.R.; Navarro-Vázquez, A.; Lei, X.X.; Gao, J.M. Herpotrichones A and B, two intermolecular [4+2] adducts with anti-neuroinflammatory activity from a *Herpotrichia* Species. *Org. Lett.* **2020**, *22*, 405–409. [CrossRef] [PubMed]
4. Yoiprommarat, S.; Unagul, P.; Suvannakad, R.; Klaysuban, A.; Suetrong, S.; Bunyapaiboonsri, T. Eremophilane sesquiterpenes from the mangrove fungus BCC 60405. *Phytochem. Lett.* **2019**, *34*, 84–90. [CrossRef]
5. Wu, W.; Dai, H.; Bao, L.; Ren, B.; Lu, J.; Luo, Y.; Guo, L.; Zhang, L.; Liu, H. Isolation and structural elucidation of proline-containing cyclopentapeptides from an endolichenic *Xylaria* sp. *J. Nat. Prod.* **2011**, *74*, 1303–1308. [CrossRef] [PubMed]
6. Xu, K.; Li, R.; Zhu, R.; Li, X.; Xu, Y.; He, Q.; Xie, F.; Qiao, Y.; Luan, X.; Lou, H. Xylarins A–D, two pairs of diastereoisomeric isoindoline alkaloids from the endolichenic fungus *Xylaria* sp. *Org. Lett.* **2021**, *23*, 7751–7754. [CrossRef] [PubMed]
7. Chen, W.; Yu, M.; Chen, S.; Gong, T.; Xie, L.; Liu, J.; Bian, C.; Huang, G.; Zheng, C. Structures and biological activities of secondary metabolites from *Xylaria* spp. *J. Fungi* **2024**, *10*, 190. [CrossRef]
8. Han, W.B.; Zhai, Y.J.; Gao, Y.; Zhou, H.Y.; Xiao, J.; Pescitelli, G.; Gao, J.M. Cytochalasins and an abietane-type diterpenoid with allelopathic activities from the endophytic fungus *Xylaria* species. *J. Agric. Food. Chem.* **2019**, *67*, 3643–3650. [CrossRef]
9. Jia, S.; Li, J.; Li, J.; Su, X.; Li, X.N.; Yao, Y.; Xue, Y. Anti-neuroinflammatory activity of new naturally occurring benzylated hydroxyacetophenone analogs from the endophytic fungus *Alternaria* sp. J030. *Chem. Biodivers.* **2022**, *19*, e202200751. [CrossRef] [PubMed]
10. Jia, S.; Su, X.; Yan, W.; Wu, M.; Wu, Y.; Lu, J.; He, X.; Ding, X.; Xue, Y. Acorenone C: A new spiro-sesquiterpene from a mangrove-associated fungus, *Pseudofusicoccum* sp. J003. *Front. Chem.* **2021**, *9*, 780304. [CrossRef] [PubMed]
11. Wu, Y.; Su, X.; Lu, J.; Wu, M.; Yang, S.Y.; Mai, Y.; Deng, W.; Xue, Y. In Vitro and in silico analysis of phytochemicals from *Fallopia dentatoalata* as dual functional cholinesterase inhibitors for the treatment of Alzheimer's disease. *Front. Pharmacol.* **2022**, *13*, 905708. [CrossRef] [PubMed]
12. Yang, W.W.; Lu, L.W.; Zhang, X.Q.; Bao, S.S.; Cao, F.; Guo, Z.Y.; Deng, Z.S.; Proksch, P. Xylariaopyrones E-I, five new α-pyrone derivatives from the endophytic fungus *Xylariales* sp. (HM-1). *Nat. Prod. Res.* **2022**, *36*, 2230–2238. [CrossRef] [PubMed]
13. Yamamoto, I.; Tai, A.; Fujinami, Y.; Sasaki, K.; Okazaki, S. Synthesis and characterization of a series of novel monoacylated ascorbic acid derivatives, 6-*O*-Acyl-2-*O*-α-D-glucopyranosyl-L-ascorbic acids, as skin antioxidants. *J. Med. Chem.* **2002**, *45*, 462–468. [CrossRef] [PubMed]
14. Zhao, Q.; Wang, C.X.; Yu, Y.; Wang, G.Q.; Zheng, Q.C.; Chen, G.D.; Lian, Y.Y.; Lin, F.; Guo, L.D.; Gao, H. Nodulisporipyrones A-D, new bioactive α-pyrone derivatives from *Nodulisporium* sp. *J. Asian Nat. Prod. Res.* **2015**, *17*, 567–575. [CrossRef] [PubMed]
15. Lichtenthaler, F.W.; Martin, D.; Weber, T.; Schiweck, H. Studies on Ketoses, 7–5-(α-D-Glucosyloxymethyl)furfural: Preparation from isomaltulose and exploration of its ensuing chemistry. *Eur. J. Org. Chem.* **1993**, *9*, 967–974. [CrossRef]
16. Miyazawa, M.; Nankai, H.; Kameoka, H. Biotransformation of (–)-α-bisabolol by plant pathogenic fungus, *Glomerella cingulata*. *Phytochemistry* **1995**, *40*, 69–72. [CrossRef]
17. Xu, J. The Preparation Method and Application of a Pyranoid Compound with Immunosuppressive Activity. CN 108913731 16 November 2021.
18. Cook, L.; Ternai, B.; Ghosh, P. Inhibition of human sputum elastase by substituted 2-pyrones. *J. Med. Chem.* **1987**, *30*, 1017–1023. [CrossRef] [PubMed]
19. Guo, Z.Y.; Lu, L.W.; Bao, S.S.; Liu, C.X.; Deng, Z.S.; Cao, F.; Liu, S.P.; Zou, K.; Proksch, P. Xylariaopyrones A-D, four new antimicrobial α-pyrone derivatives from endophytic fungus *Xylariales* sp. *Phytochem. Lett.* **2018**, *28*, 98–103. [CrossRef]

20. Zhang, H.; Deng, Z.; Guo, Z.; Peng, Y.; Huang, N.; He, H.; Tu, X.; Zou, K. Effect of culture conditions on metabolite production of *Xylaria* sp. *Molecules* **2015**, *20*, 7940–7950. [CrossRef] [PubMed]
21. Tian, J.F.; Yu, R.J.; Li, X.X.; Gao, H.; Guo, L.D.; Tang, J.S.; Yao, X.S. ^{1}H and ^{13}C NMR spectral assignments of 2-pyrone derivatives from an endophytic fungus of sarcosomataceae. *Magn. Reson. Chem.* **2015**, *53*, 866–871. [CrossRef] [PubMed]
22. Pérez-Castorena, A.L.; Arciniegas, A.; Guzmán, S.L.; Villaseñor, J.L.; Vivar, A.R. Eremophilanes from *Senecio mairetianus* and some reaction products. *J. Nat. Prod.* **2006**, *69*, 1471–1475. [CrossRef] [PubMed]
23. Arora, D.; Sharma, N.; Singamaneni, V.; Sharma, V.; Kushwaha, M.; Abrol, V.; Guru, S.; Sharma, S.; Gupta, A.P.; Bhushan, S.; et al. Isolation and characterization of bioactive metabolites from *Xylaria psidii*, an endophytic fungus of the medicinal plant *Aegle marmelos* and their role in mitochondrial dependent apoptosis against pancreatic cancer cells. *Phytomedicine* **2016**, *23*, 1312–1320. [CrossRef] [PubMed]
24. Hallock, Y.F.; Clardy, J.; Kenfield, D.S.; Strobel, G. De-*O*-methyldiaporthin, a phytotoxin from *Drechslera siccans*. *Phytochemistry* **1988**, *27*, 3123–3125. [CrossRef]
25. Feng, C.C.; Chen, G.D.; Zhao, Y.Q.; Xin, S.C.; Li, S.; Tang, J.S.; Li, X.X.; Hu, D.; Liu, X.Z.; Gao, H. New isocoumarins from a cold-adapted fungal strain *Mucor* sp. and their developmental toxicity to zebrafish embryos. *Chem. Biodivers.* **2014**, *11*, 1099–1108. [CrossRef]
26. Lin, Y.; Wu, X.; Feng, S.; Jiang, G.; Zhou, S.; Vrijmoed, L.L.P.; Jones, E.B.G. A novel *N*-cinnamoylcyclopeptide containing an allenic ether from the fungus *Xylaria* sp. (strain #2508) from the South China Sea. *Tetrahedron Lett.* **2001**, *42*, 449–451.
27. Bruhn, T.; Schaumloffel, A.; Hemberger, Y.; Bringmann, G. SpecDis: Quantifying the Comparison of Calculated and Experimental Electronic Circular Dichroism Spectra. *Chirality* **2013**, *25*, 243–249. [CrossRef] [PubMed]
28. Zhang, N.; Shi, Z.; Guo, Y.; Xie, S.; Qiao, Y.; Li, X.N.; Xue, Y.; Luo, Z.; Zhu, H.; Chen, C.; et al. The absolute configurations of hyperilongenols A–C: Rare 12,13-seco-spirocyclic polycyclic polyprenylated acylphloroglucinols with enolizable β, β′-tricarbonyl systems from *Hypericum longistylum* Oliv. *Org. Chem. Front.* **2019**, *6*, 1491–1502. [CrossRef]
29. Wu, Y.; Xie, S.; Hu, Z.; Wu, Z.; Guo, Y.; Zhang, J.; Wang, J.; Xue, Y.; Zhang, Y. Triterpenoids from whole plants of *Phyllanthus urinaria*. *Chin. Herb. Med.* **2017**, *9*, 193–196. [CrossRef]
30. Ma, Y.Y.; Zhao, D.G.; Zhou, A.Y.; Zhang, Y.; Du, Z.; Zhang, K. α-Glucosidase inhibition and antihyperglycemic activity of phenolics from the flowers of *Edgeworthia gardneri*. *J. Agric. Food. Chem.* **2015**, *63*, 8162–8169. [CrossRef]